A calibration procedure for the prediction of thermo-acoustic instabilities with a low-order model in a gas-turbine burner

Matteo Bargiacchi, Anaïs Guaus[*], Julien Favier[†], Alessandro Bottaro
DICCA, Università di Genova,
Via Montallegro 1, 16145 Genova, Italy

Ezio Cosatto, Giulio Mori
Ansaldo Energia,
Corso F. Perrone 118,
16161 Genova, Italy

Low level of pollutants can be achieved by lean and premixed burning. Unfortunately, these are the conditions at which the undesirable phenomenon of self-excited thermo-acoustic oscillations occurs. These are responsible for inefficient burning and structural stresses so intense that they can lead to engine and combustor failure. Understanding these phenomena is an important goal of designers and theoreticians. Large Eddy Simulations of the complete governing equations and finite elements solutions of the acoustic equations in realistic domains are useful to describe the phenomenon and have enjoyed much popularity in recent years; such techniques are however not flexible enough to allow extensive parametric studies during a preliminary design phase. A lumped, linear model is developed and implemented here, and computations are carried out to highlight the effect of the most important parameters of the problem. To validate the results a calibration is conducted on the basis of reference three-dimensional finite elements simulations. Guidelines on the choice of geometrical parameters for the lumped model are given. Additionally, a new model describing the flame interactions with the acoustic field is developed and tested.

Nomenclature

A_j Cross sectional area of duct j
A_n^+ Amplitude of the clockwise (downstream travelling if $n=0$) acoustic perturbation of the n^{th} azimuthal mode
A_n^- Amplitude of the counter-clockwise (upstream travelling if $n=0$) acoustic perturbation of the n^{th} azimuthal mode
A_n^e Amplitude of the entropy wave of the n^{th} azimuthal mode
c_s Speed of sound
d_j Thickness of duct j
f Frequency $[Hz]$
GR Growth Rate $[1/s]$
H Total enthalpy $[m^2/s^2]$
i Imaginary unit
J_n Bessel function of the first kind of order n
L_j Length of duct j
$\dot{m}$ Mass flow rate
M Mach number
PM Molecular Mass $[Kg/mol]$
N_b Number of burners
p Pressure
q Volumetric heat release rate $[W/m^3]$
Q Rate of heat release per unit of area $[W/m^2]$
R Perfect Gas constant: $R=R(T)$ $[J/Kg\cdot K]$
R_j Radius of duct j
S Entropy density $[J/Kg\cdot K]$
t Time
T Temperature
$\mathbf{v}$ Velocity vector
u Axial velocity
v Radial velocity
w Azimuthal velocity
Y_n Bessel function of the second kind of order n

γ Ratio of specific heats: $\gamma=\gamma(T)$
ρ Mass density
τ Time delay
ω Angular frequency $[rad/s]$

$(..)_1$ *Plenum*

[*]Present address: INRA, Centre de Montpellier, Unité Eco&Sols, 2 place Viala, 34060 Montpellier Cedex 1, France
[†]Present address: CIEMAT, Av. Complutense 22, 28040 Madrid, Spain

$(..)_2$ Premixer
$(..)_{2b}$ *CBO*'s
$(..)_3$ Combustion Chamber
$\bar{}$ mean quantity
$'$ fluctuating quantity

1 Introduction

Thermo-acoustic instabilities may occur whenever combustion takes place inside a resonator. The phase difference between heat release oscillations and pressure waves arriving at the fuel injection points is responsible for the phenomenon, as described by Lord Rayleigh [1]. Strong vibrations at low frequencies may occur inside the resonator causing the humming phenomenon that irremediably affects the functioning and the efficiency of the system. Integral principles are useful to understand the nature of humming and could be implemented in three-dimensional simulations. Unfortunately, parametric studies carried out on the basis of these simulations for geometries characterizing, e.g., the combustion chambers of gas turbines, are very expensive and there is no straightforward way to modify the resonator's geometry in order to mitigate or eliminate thermo-acoustic oscillations. In this paper, a lumped model of a real gas turbine combustor is proposed. The present approach represents a very fast way to analyze the stability of the system under consideration; it constitutes a very light tool which can be quickly adapted to study several operating conditions and geometries. This tool, a low-order-model, hereinafter referred to as LOM, finds the complex eigenvalues of the linear stability operator of the system. Because of the linear approximation, no information on the amplitude of the resulting eigenfunctions is available: a LOM is thus only able to predict whether a mode might evolve towards a limit cycle. In the past, low order thermo-acoustic linear models have been described by Dowling & Stow [2], Schuermans [3], Sattelmayer [4], Evesque & Polifke [5], Rumsey et al. [6], Morgan & Stow [7] and Bellucci et al. [8]. Our model builds upon their contributions; although we could omit mathematical details of the approach followed, we prefer, for the sake of completeness, to provide a reasonably complete account of the LOM developed.

LOM's are generally based on conservation principles to be enforced at the junction of neighbouring duct, together with boundary conditions and constitutive relations. Any lumped model inevitably requires a calibration against simulations or experiments obtained in more realistic geometries: this is one of the objective of the present paper and it is described in section 3. A brief analysis of the effect of a non-zero mean flow is addressed in section 4. In order to close the problem a model representing the heat release mechanism of the unsteady flame is required: a so-called Flame Transfer Function (FTF) is often used to describe the flame dynamics. Unfortunately, it is very easy to negatively affect the response of the system by the choice of a wrong or incomplete FTF, possibly modifying the stability characteristics. Typical transfer functions [9] contain at least two unknown parameters, on whose choice the phenomena predicted by the model strongly depend. In section 5, a new model for the flame dynamics is proposed.

2 The physical model and the equations

The basic idea is to analyse the combustor of a gas turbine through a set of equations suited to represent the state of the system. The internal variables are the smallest possible subset of system variables that can represent the entire state of the system at any given time; they are expressed as vectors. The differential and algebraic equations that describe the linear system are written in matrix form. The number of unknown variables (i.e. the length of the associated vector) must be equal to the number of equations (i.e. to the rank of the relative matrix) in order to have a well-posed problem. Sometimes, and this is the case here, the equations available are less than the number required so that transfer functions, coupling two or more variables, become necessary. It is important to stress the fact that using a transfer function may cause the loss of internal information of the system, affecting its stable/unstable nature.

Variables for an annular gas turbine are the perturbations thermodynamic and mechanical quantities such as pressure, velocity or heat release. The whole system is modelled as a network of different ducts: an annular diffuser at the compressor's exit, N_b axial premixers, and an annular combustion chamber, before the inlet of the turbine. At the end of the cylindrical premixers, N_{CBO} Cylindrical Burner Outlets ($CBO's$) might be positioned; their function is that of disrupting the axisymmetry of the system to modify both the shape of the flame and the time a disturbance released at the injector takes to reach the flame front.

2.1 Mean flow

Every variable $G(x,r,\theta,t)$ is decomposed into a mean value $\bar{G}$, constant in each duct, and a fluctuating value $G'(x,r,\theta,t)$, with $G' << \bar{G}$. The LOM requires a preliminary computation of the mean flow parameters. Since it is based on a lumped approach, only a mean pressure $\bar{p}$, axial velocity $\bar{u}$, temperature $\bar{T}$ and density $\bar{\rho}$ are to be computed in each duct, together with the rate of heat release per unit area Q supplied by the flame. Since all the premixers and the *CBO*'s are alike, the number of unknowns is always $N^{mean} = 17$ (4 unknowns for the compressor diffuser, usually called *plenum*, the premixing ducts, the *CBO*'s and the combustion chamber together with the heat release).

The conservation principles used to calculate both the mean and perturbed variables are applied locally for each burner. For this purpose, *plenum* and combustion chamber need to be divided into N_b sectors. Since the premixers are equally spaced, the sectors are centred around each premixer, i.e. around the angle

$$\theta_i = \frac{2\pi}{N_b}(i-1), \quad 1 \le i \le N_b,$$

respectively, and with identical sections βA_1 in the *plenum*

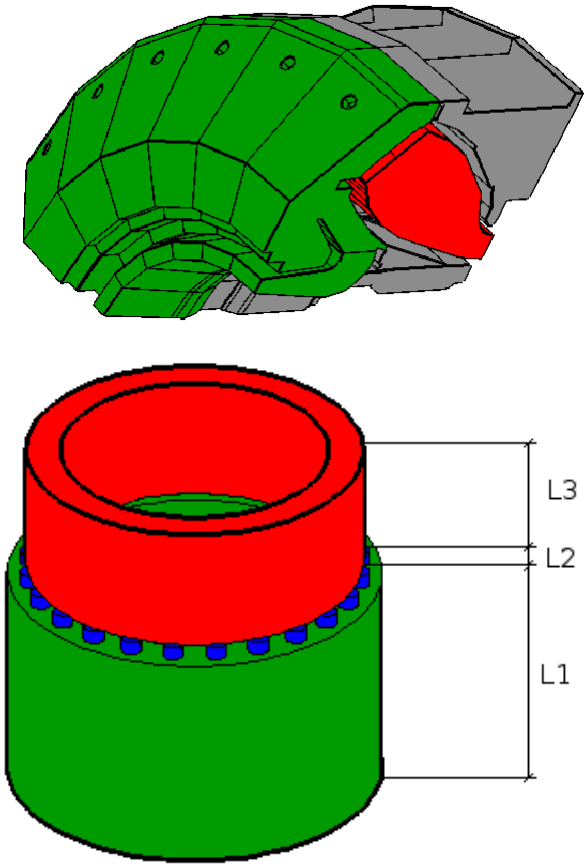

Fig. 1. (Top) A quarter of the real geometry. (Bottom) LOM's outline. The *plenum*, is colored in green, premixers (not visible in the real geometry) in blue and the combustion chamber in red. *CBO*'s are not shown here.

and βA_3 in the chamber, where

$$\beta = 1/N_b.$$

As clearly noticeable from figure 1, only a part of the *plenum* can be modelled since the LOM is able to represent only the segment between the compressor outlet and the premixers inlet, disregarding the volumes where film cooling takes place (colored in grey).

A perfect gas equation is written in each duct providing 4 equations, one each for *plenum*, premixers, *CBO*'s and combustion chamber:

$$\bar{p} = \bar{\rho} R \bar{T}.$$

The mass flux conservation, written locally at each premixer inlet, imposes:

$$\beta \bar{\dot{m}}_1 = \bar{\dot{m}}_2.$$

At the interface of the premixers with the *CBO*'s it becomes:

$$\bar{\dot{m}}_2 = \bar{\dot{m}}_{2b},$$

and at the combustion chamber inlet it reads:

$$\bar{\dot{m}}_3 = \bar{\dot{m}}_1.$$

The energy conservation between the *plenum* and the premixers yields:

$$\beta \bar{\dot{m}}_1 \bar{H}_1 = \bar{\dot{m}}_2 \bar{H}_2,$$

with H the total enthalpy defined as $\bar{H} = c_P \bar{T} + \bar{u}^2/2$. Between a premixer and the corresponding *CBO* it is:

$$\bar{\dot{m}}_2 \bar{H}_2 = \bar{\dot{m}}_{2b} \bar{H}_{2b}.$$

and at the combustion chamber inlet the following expression holds:

$$\bar{\dot{m}}_3 \bar{H}_3 = \bar{\dot{m}}_1 \bar{H}_1 + A_3 Q.$$

2.1.1 Isentropic/grid conditions

The turbine configuration generally includes a grid at each premixer inlet. Its influence is neglected in the present computation, so that an isentropic condition [2], might be applied:

$$\bar{p}_1/\bar{p}_2 = (\bar{\rho}_1/\bar{\rho}_2)^{\gamma};$$

if the grid had been considered, the following grid-type equation could have been employed:

$$\bar{p}_1 - \bar{p}_2 = \frac{1}{2} k_{12} \bar{\rho}_2 \bar{u}_2^2,$$

with k_{12} an empirical loss parameter [10]. For the purposes of the present paper the grid condition is irrelevant: it is however interesting to observe that its application has a remarkable influence on stability when dealing with simplified configurations where axial waves, established downstream of the grid, assume major relevance. This is the case of test rigs with a single burner where the typical azimuthal waves of the annular combustion chamber are not present [11].

2.1.2 "Borda" equations

At each *CBO* inlet (where there is a sudden area increase) a Borda-like equation [12] should be implemented:

$$\bar{\dot{m}}_2 \bar{u}_2 - \bar{\dot{m}}_{2b} \bar{u}_{2b} = A_{2b} \left(\bar{p}_{2b} - \bar{p}_2 \right),$$

and a similar equation holds for the set of premixers/*CBO*'s reaching the combustion chamber:

$$\bar{\dot{m}}_3 \bar{u}_3 - \sum_{k=1}^{Ncbo} \bar{\dot{m}}_{2b}^k \bar{u}_{2b}^k - \sum_l \bar{\dot{m}}_2^l \bar{u}_2^l = \beta A_3 \left(\sum_{k=1}^{Ncbo} \bar{p}_{2b}^k + \sum_l \bar{p}_2^l \right) - A_3 \bar{p}_3,$$

where $l \leq N_b$ is the index of the burners which do not terminate with *CBO*'s.

The total number of equations is then 13, and to close the system it is sufficient to have 4 input data, for instance pressure, temperature and mass flux in the *plenum* along with the flame temperature.

2.2 Disturbance flow

The convective inhomogeneous wave equation for disturbances is, for speed of sound c_s assumed constant,

$$\frac{D^2p'}{Dt^2} - c_s^2\nabla^2 p' = (\gamma-1)\frac{Dq'}{Dt}, \tag{1}$$

where $D/Dt = \partial/\partial t + \bar{\mathbf{v}}\cdot\nabla$. Equation (1) is solved with the right hand side evaluated in a thin sheet at or near the combustion chamber inlet. Separating each perturbation in acoustic and entropy contributions, general expressions in cylindrical coordinates can be deduced, obtaining a superposition of axial, azimuthal and radial waves. Since the premixers have small radii, only axial waves are assumed to propagate through them. The contribution of entropy is accounted for, so that the LOM is coherent with the integral principles proposed in [13]:

$$\int_\Omega (\frac{T'q'}{\bar{T}} - \frac{\bar{p}}{Rc_p}S'\mathbf{v}'\cdot\nabla\bar{S})dV > \cancel{\int_\Sigma p'\mathbf{v}'\cdot d\mathbf{A}},$$

where the net flux of acoustic energy lost through the boundary Σ of the system can be neglected. This hypothesis is confirmed by experience and it is conservative since it assumes the worst possible condition. Furthermore, numerical results confirm that the entropy-related term in the equation above is not negligible and potentially much larger than the acoustic contribution [13].

The final form of axially-propagating disturbances in the premixers is [5]:

$$\begin{aligned}
p' &= \left(A^+ e^{ik^+x} + A^- e^{ik^-x}\right)e^{i\omega t},\\
\rho' &= \frac{1}{\overline{c}^2}\left(A^+ e^{ik^+x} + A^- e^{ik^-x} - A^e e^{ik^0x}\right)e^{i\omega t},\\
u' &= -\frac{1}{\overline{\rho}}\left(\frac{k^+}{\alpha^+}A^+ e^{ik^+x} + \frac{k^-}{\alpha^-}A^- e^{ik^-x}\right)e^{i\omega t},\\
T' &= \frac{1}{c_p\overline{\rho}}\left[\left(A^+ e^{ik^+x} + A^- e^{ik^-x}\right) + \frac{1}{\gamma-1}A^e e^{ik^0x}\right]e^{i\omega t},
\end{aligned} \tag{2}$$

with

$$\begin{cases}
k^\pm = \dfrac{M\omega \mp |\omega^2|}{\overline{c}(1-M^2)},\\
k^0 = -\dfrac{\omega}{\overline{u}},\\
\alpha^\pm = \omega + \overline{u}k^\pm.
\end{cases}$$

In the *plenum* and combustion chamber, to account for the possible asymmetry of the geometry (for example when a few *CBO*'s are present), the perturbation is a combination of $N_n = N_b$ (even) azimuthal modes:

$$\begin{aligned}
p' &= \sum_{n=-N_n/2+1}^{N_n/2}\left(A_n^\pm e^{ik^\pm x}\right)B_{n,m}(r)\,\Omega,\\
\rho' &= \sum_{n=-N_n/2+1}^{N_n/2}\frac{1}{\overline{c}^2}\left[\left(A_n^\pm e^{ik^\pm x}\right)B_{n,m}(r) - A_n^e e^{ik^0x}E(r)\right]\Omega,\\
u' &= \sum_{n=-N_n/2+1}^{N_n/2} -\frac{1}{\overline{\rho}}\left(\frac{k^\pm}{\alpha^\pm}A_n^\pm e^{ik^\pm x}\right)B_{n,m}(r)\,\Omega,\\
v' &= \sum_{n=-N_n/2+1}^{N_n/2}\frac{i}{\overline{\rho}}\left(\frac{1}{\alpha^\pm}A_n^\pm e^{ik^\pm x}\right)\frac{dB_{n,m}(r)}{dr}\,\Omega,\\
w' &= \sum_{n=-N_n/2+1}^{N_n/2} -\frac{n}{r\overline{\rho}}\left(\frac{1}{\alpha^\pm}A_n^\pm e^{ik^\pm x}\right)B_{n,m}(r)\,\Omega,\\
T' &= \sum_{n=-N_n/2+1}^{N_n/2}\frac{1}{c_p\overline{\rho}}\left[\left(A_n^\pm e^{ik^\pm x}\right)B_{n,m}(r) + \frac{E(r)}{\gamma-1}A_n^e e^{ik^0x}\right]\Omega,
\end{aligned} \tag{3}$$

where

$$\begin{cases}
k^\pm = k_{n,m}^\pm = \dfrac{M\omega \mp \sqrt{\omega^2 - \chi_{n,m}^2\overline{c}^2(1-M^2)}}{\overline{c}(1-M^2)},\\
k^0 = -\dfrac{\omega}{\overline{u}},\\
\alpha^\pm = \alpha_{n,m}^\pm = \omega + \overline{u}k_{n,m}^\pm,\\
A_n^\pm e^{ik^\pm x} = A_n^+ e^{ik^+x} + A_n^- e^{ik^-x},\\
\Omega = e^{i\omega t + in\theta},
\end{cases}$$

with n and m the azimuthal and radial wave numbers, respectively. In the most general case $\chi_{n,m}$ is the $(m+1)^{th}$ solution of $\frac{dY_n}{dr}(\chi_{n,m}R_{j,outer})\frac{dJ_n}{dr}(\chi_{n,m}R_{j,inner}) - \frac{dJ_n}{dr}(\chi_{n,m}R_{j,outer})\frac{dY_n}{dr}(\chi_{n,m}R_{j,inner}) = 0$, in the annular ducts, with J_n and Y_n the Bessel functions of the first and second kind, respectively. The function $E(r)$ is arbitrary and

$$\begin{aligned}
B_{n,m}(r) = &\frac{dY_n}{dr}(\chi_{n,m}R_{j,outer})J_n(\chi_{n,m}r)\\
&-\frac{dJ_n}{dr}(\chi_{n,m}R_{j,outer})Y_n(\chi_{n,m}r)
\end{aligned} \tag{4}$$

in both the annular ducts.

2.2.1 Mass flux conservation equations

As the perturbation in the *plenum* depends on both θ and r, the local mass flux conservation equation at each burner inlet becomes[1]

$$\int_{R_{1inner}}^{R_{1outer}}\int_{\theta^i-\pi\beta}^{\theta^i+\pi\beta}(\rho_1 u_1)'\,r dr d\theta = \left(\dot{m}_2^i\right)', \tag{5}$$

[1] $R_{j,inner} = R_j - d_j/2$ and $R_{j,outer} = R_j + d_j/2$

for $1 \le i \le N_b$, at $x = L_1$, and at each burner outlet:

$$\int_0^{R_3} \int_{\theta^i - \pi\beta}^{\theta^i + \pi\beta} (\rho_3 u_3)' \, r dr d\theta = \left(\dot{m}_2^i\right)', \tag{6}$$

for $1 \le i \le N_b$, at $x = L_1 + L_2$.

2.2.2 Energy conservation equations

As for the mass flux, a disturbance energy conservation equation at each burner inlet is written locally:

$$\int_{R_{1inner}}^{R_{1outer}} \int_{\theta^i - \pi\beta}^{\theta^i + \pi\beta} (\rho_1 u_1 H_1)' \, r dr d\theta = \left(\dot{m}_2^i H_2^i\right)', \tag{7}$$

for $1 \le i \le N_b$, at $x = L_1$, and at each burner outlet:

$$\int_0^{R_3} \int_{\theta^i - \pi\beta}^{\theta^i + \pi\beta} (\rho_3 u_3 H_3)' \, r dr d\theta = \left(\dot{m}_2^i H_2^i\right)' + \beta S_3 \left(Q^i\right)', \tag{8}$$

with $1 \le i \le N_b$, at $x = L_1 + L_2$.

2.2.3 Isentropic conditions

A linearised isentropic condition applies at each burner inlet:

$$\left(p_1 / p_2^i\right)' = \left(\left(\rho_1 / \rho_2^i\right)^\gamma\right)', \quad 1 \le i \le N_b, \tag{9}$$

at $x = L_1 + L_2$, $\theta = \theta_i$, $r = (R_{1inner} + R_{1outer})/2$. Should a grid be present, the corresponding condition on disturbances can be easily ascertained from the second formula in section 2.1.1.

2.2.4 "Borda" equations

The Borda-like equations used at the burners outlet are the linearized forms of those used for the mean flow, i.e.:

$$\left(\dot{m}_2^i u_2^i\right)' + \beta S_3 \, p_2' = \int_0^{R_3} \int_{\theta^i - \pi\beta}^{\theta^i + \pi\beta} \left[\left(\rho_3 u_3^2\right)' + p_3'\right] r dr d\theta, \quad 1 \le i \le N_b, \tag{10}$$

at $x = L_1 + L_2$.

2.2.5 Inlet/outlet conditions

Whichever boundary condition is used, it is verified independently by each mode and thus $2N_n$ inlet conditions and N_n outlet conditions are needed. Once the acoustic impedance $\zeta = p'/u'$ is defined, the boundary conditions can either prescribe a specific value of ζ (for example $\zeta = 0$ at an open end or $\zeta \to \infty$ at a solid wall), or specify, for example, that the given outflow boundary is choked, in which case $\rho'/\bar{\rho} + 2u'/\bar{u} - \gamma p'/\bar{p} = 0$ [14], correct to first order even in the presence of circumferentially-varying waves [15]. At the inlet a further relation must be provided. A condition imposing the absence of entropy waves at the compressor outlet [2] is:

$$\frac{p'}{\bar{p}} - \frac{\rho'}{\bar{\rho}} + (\gamma - 1) M_1 \frac{u'}{\bar{u}} = 0. \tag{11}$$

2.2.6 Other boundary conditions

The missing conditions for the azimuthal and radial waves are those of periodicity $v'(\theta) = v'(\theta + 2\pi)$ plus the enforcement of $w' = 0$ at the radial boundaries of the main ducts $r = R_{inner}$ and $r = R_{outer}$.

2.2.7 Flame transfer function

To close the problem, a model able to represent the unsteady heat release mechanism for each burner is required, often in the form of a flame transfer function, such as:

$$\frac{Q'}{\bar{Q}} = \sum_i \frac{G_i'}{\bar{G}_i} F_i(\omega)$$

where G_i is a thermodynamic variable involved in the combustion process and Q is the rate of heat release per unit area. A discussion on this is postponed until section 5. The heat release is confined in a thin sheet at the combustion chamber inlet, hence no spatial dependence of Q' is expected,

$$Q'(t) = \hat{Q} e^{i\omega t}, \tag{12}$$

with $\hat{Q}$ an amplitude coefficient.

2.2.8 Explicit form of the mass flux conservation equation

In order to show the contribution of the radially dependent terms, the mass flux conservation equations are explicitly written as an example. Using equations (2) and (3), the mass flux conservation equations (5) and (6) become

$$\sum_n I_{in} \left[\Upsilon_{n,m}^+ K_{nm} A_n^+ + \Upsilon_{n,m}^- K_{nm} A_n^- - \frac{\overline{u}_d}{\overline{c}_d^2} K_{nm}^e A_n^e\right] = A_2 \left[\Upsilon_2^+ A_2^+ + \Upsilon_2^- A_2^- - \frac{\overline{u}_2}{\overline{c}_2^2} A_2^e\right], \quad 1 \le i \le N_b,$$

at $x = L^d$, where $d = 1$ refers to the *plenum* and $d = 3$ to the chamber, using $L^1 = L_1$ and $L^2 = L_1 + L_2$, and

$$\Upsilon_{n,m}^\pm = \left(\frac{\overline{u}_d}{\overline{c}_d^2} - \frac{k_{n,m}^\pm}{\alpha_{n,m}^\pm}\right), \quad \Upsilon_2^\pm = \left(\frac{\overline{u}_2}{\overline{c}_2^2} - \frac{k_2^\pm}{\alpha_2^\pm}\right).$$

The azimuthal dependence is reduced to the integral:

$$I_{in} = \int_{\theta^i - \pi\beta}^{\theta^i + \pi\beta} e^{in\theta} d\theta = \begin{cases} \frac{2}{n} e^{in\theta^i} sin(n\beta\pi), & n \neq 0 \\ 2\beta\pi, & n = 0 \end{cases},$$

$$1 \leq i \leq N_b,$$

and the radial contribution is included in terms K_{nm} for acoustic waves and K^e_{nm} for entropy waves. The integral K_{nm} is

$$K_{nm} = \int_{R_{inner}}^{R_{outer}} B_{n,m}(r) r dr,$$

where $B_{n,m}$ is defined by equation (4) and (R_{inner}, R_{outer}) is equal to (R_{1i}, R_{1o}) for the *plenum* and $(0, R_3)$ for the combustion chamber. The integral K^e_{nm} is defined as

$$K^e_{nm} = K^e = \int_{R_{inner}}^{R_{outer}} E(r) r dr,$$

in which the arbitrary function $E(r)$ is fixed to unity in both the *plenum* and the chamber. Setting $E(r)$ does not influence the solution of the system; however, it affects the resulting mode shapes since it defines the ratio between the amplitudes of acoustic and entropy waves.

2.2.9 The final matrix of the system

Combining equations (2-12), choosing the proper boundary conditions and setting the flame transfer function, a well posed linear problem is obtained:

$$[\mathbf{M}(\omega)] \cdot \begin{Bmatrix} A^+_n \\ A^-_n \\ A^e_n \\ \hat{Q} \end{Bmatrix} = \mathbf{0}; \tag{13}$$

this homogeneous system of equations has a non-trivial solution when $det[\mathbf{M}] = 0$. The problem is to obtain the complex values of $\omega = \omega_r + i\omega_i$ that render the determinant equal to zero, and this is accomplished by a quick graphical approach by looking at the points of intersection of isolines of zero real part and zero imaginary part of the determinant. Henceforth, $f = \omega_r/2\pi$ represents the frequency of the mode of oscillation, and $GR = -\omega_i$ defines whether the mode is unstable or not. A positive value of the growth rate *GR* means that an unstable mode exists which might bring the whole system out of equilibrium towards a new state characterized by limit cycle oscillations.

3 Calibration of the system for acoustic modes

The LOM is based on a lumped approach and a direct link with a more realistic configuration must be found. In the first stage of the analysis the main parameters to be calibrated are geometrical. Length, radius and thickness of the LOM ducts cannot be set in a straightforward way, when examining the full three-dimensional model; it has thus been decided that all geometrical parameters in the LOM, such as the length of a duct or its mean radius, must match acoustically corresponding values in the real geometry. A calibration against a three-dimensional finite element acoustic simulation (3DFEA), able to catch all the stable or unstable resonant modes, is thus required. The aim here is to provide guidelines on the choice of the geometrical parameters when reference results are not available.

As a rule of thumb, the larger the dimension, the smaller the frequency of the waves established in a duct. Since humming arises at relatively low frequencies, the dangerous waves are presumably those (standing or travelling) in the longer ducts, i.e. the *plenum* and the combustion chamber. The waves in the premixers are axial and are detected only for frequencies larger than the potentially dangerous ones. Therefore, the *plenum* and the combustion chamber will be hereinafter referred to as the *main ducts*. In the annular configuration of the combustion chamber there are eight parameters to be set[2] and, at first glance, only an automatic optimization procedure seems to be able to provide a solution to this problem. While it would be an interesting challenge to create an automatic tool to simultaneously match all lengths, frequencies and mode types, between the LOM and the three-dimensional acoustic tool, it is possible to converge rapidly with the iterative approach outlined below.

To start with, the effect of the flame and the transport of gas through the system are discarded, and the approach aims at matching LOM with 3DFEA results on the hypothesis that the mean flow velocity $\bar{u}$ in each duct and the flame disturbance Q' vanish. In this calibration phase the presence of *CBO*'s is not considered; the geometry is thus axisymmetric and each azimuthal mode appears as a double solution in the complex ω plane. In this phase, searching for conditions which guarantee acoustic equivalence between the 3DFEA and the LOM is carried out for the parameters summarized in table 1. For simplicity, solid wall boundary conditions are imposed at the beginning and at the end of the main ducts in both the LOM and the 3DFEA configurations; for the latter case results are available [16, 17].

A preliminary low order simulation is needed in order to step in the algorithm displayed in the flowchart 2. Such a simulation should be carried out with tentative geometrical values chosen on the basis of experience and common sense. Once the first step is carried out a first comparison between the results is possible. Since coupling among modes does not arise, pure tones are easily recognizable with either approach; for instance, a n=2 mode in the combustion chamber, or a n=4 mode in the *plenum*, can be identified immediately, since the azimuthal wave-number n represents the number of peaks or valleys (maxima or minima) in the distribution of p'

[2] Length L_1, mean radius R_1 and thickness d_1 of the *plenum*; length L_3, mean radius R_3 and thickness d_3 of the combustion chamber, plus length L_2 and cross sectional area A_2 of the premixing ducts.

Table 1. Input parameters for the calibration phase

Inlet temperature	$683\,K$
Inlet pressure	$16\,bar$
Flame temperature	$1736\,K$
Mass flow rate	0
Boundary conditions	$u' = 0$
No flame perturbations	$Q' = 0$

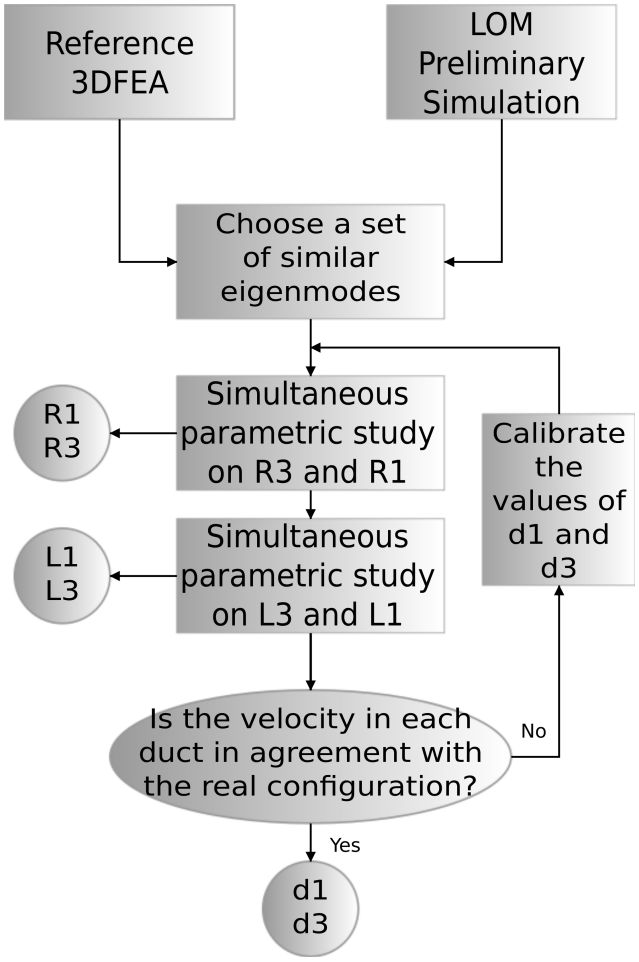

Fig. 2. Flowchart describing the steps needed for the calibration algorithm: preliminary simulations, parametric investigations and final definition of the geometry.

along the circumference. In case axisymmetry were broken (by the *CBO*'s, for example) it would be more difficult – although not impossible - to match specific modes between the LOM and the 3DFEA results.

The finite element approach provides 16 eigenvalues with frequencies up to about $0.2\,kHz$ [17]. Some of these modes correspond to disturbances confined in the inner/outer part of the *plenum* in figure 1 (in grey), so that it would be unreasonable to expect to be able to capture them with the LOM. All the important modes, however, should be captured by our model.

The procedure adopted to calibrate the geometrical values in the LOM is sketched in figure 2. After the first simulation four acoustic modes with the lowest possible frequencies are chosen: two axial and two azimuthal. The two axial modes must be established in either the *plenum*, the combustion chamber, or in both ducts. Through the choice of axial waveforms the ducts' lengths are calibrated. For the calibration of the radii the two azimuthal modes, which should also be established in either the *plenum*, the combustion chamber, or in both ducts, are focused upon. Finally, via conservation of mass, it is easy to specify the ducts' thicknesses. It is important to point out that the combustion chamber radius, R_{cc}, is sufficiently independent of the other geometrical parameters for its calibration to be carried out individually. In other words, the first thing to do is – by focusing on the azimuthal mode established in the combustion chamber – vary R_3 until the frequency found by the LOM for that particular azimuthal function corresponds to the frequency of the same waveform in the 3DFEA. The procedure for R_1 is then repeated until the corresponding azimuthal modes are matched. At this point, one of the two axial modes should be focused upon, say that which is concentrated (mainly or only) in the chamber, and L_3 is varied until the frequency of the axial mode is equal to that of the corresponding acoustic mode in the 3DFEA. The procedure to calibrate L_1 is then repeated. In doing this, it is found that the frequencies of the azimuthal modes calibrated previously change but mildly. The final step of the iteration is to set d_1 and d_3 so that the cross sectional areas of the main ducts $2\pi R_j d_j, j = 1,3$ are such that the imposed mass flow rate is satisfied. The LOM is then run and the results are compared to those of the 3DFEA. If the agreement is not satisfactory the procedure starts over. With this algorithm convergence is reached within the desired accuracy with a handful of iterations (often as few as two or three).

In the absence of reference results to compare with, the rules of thumb that have been found are summarized in table 2. The lengths (R_p, R_{cc}, L_p and L_{cc}) indicated in the table shown in figure 3.

Table 2. Rules for defining the acoustic dimensions of the main ducts of the LOM.

$R_1 \approx 0.91 R_p$	$L_1 \approx 1.17 L_p$
$R_3 \approx 0.91 R_{cc}$	$L_3 \approx 0.91 L_{cc}$

Only a limited influence on the relevant frequencies of the acoustic dimensions of the premixing ducts has been found. The distance between the fuel injection point and the flame front appears in the definition of some FTF parameters, indirectly affecting the stability.

A brief discussion of table 2 is in order: each acoustic dimension turns out to be slightly shorter than the relative real one, with the exception of the acoustic length L_1 of the

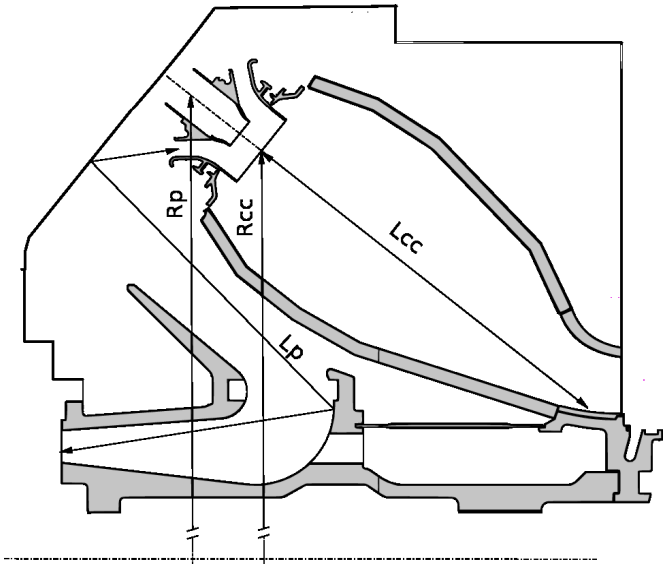

Fig. 3. Sketch of the geometry with the reference lengths used in defining the geometrical parameters of the LOM.

compressor diffuser, here called *plenum*. The radius of the *plenum* R_1 is comparable to the radial coordinate at which the burners' inlet is located. The radius of the combustion chamber R_3 is a measure of the actual radial position of the flame front rather than the position of the burners' outlet. In the same manner the acoustic length of the combustion chamber L_3 approaches the distance between the flame front and the turbine inlet. Concerning the acoustic length of the *plenum*, L_1, there is no simple relation between it and the path travelled by a particle through it, or the path of an acoustic wave. However, the exact definition of L_1 is not crucial in the understanding of phenomena, such as the the humming effect, which may occur in the burner.

At this stage the LOM geometry is well defined to match the 3DFEA results describing the acoustic modes superimposed on a realistic mean flow. Once again, the importance of the mean flow on the reliability of the results must be highlighted: its absence would deny the possibility to consider entropy waves, whose importance has been largely demonstrated (see e.g. [13]).

A comparison of the main results for the pressure mode shapes obtained with both the LOM and the 3DFEA in the absence of mean flow follows[3]. Despite the intrinsically different approaches, a very good agreement is obtained as far as the frequencies of oscillation which can possibly yield humming are concerned. All the acoustic modes obtained with the two different tools are summarized in table 3; some representative modes are shown for both the reference and the LOM results in figures 4 to 11. In general, the comparison is very satisfactory. For the sake of completeness, in figures 12 and 13 the undetected modes **1** and **11** confined in the inner part of the *plenum* are shown. Clearly such modes cannot be caught by the LOM; furthermore, they are of minor interest for the stability of the whole system.

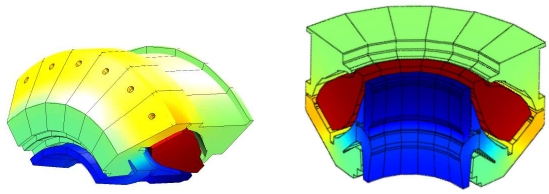

(a) (b)

Fig. 4. Pressure mode shape for the $\mathbf{3^{rd}}$ mode $n = 0$, obtained at unit dimensionless frequency with the 3DFEA code.

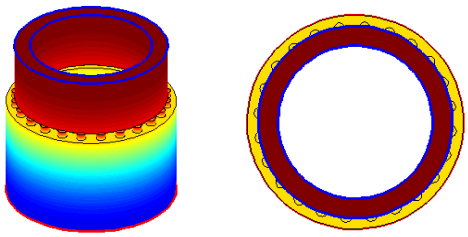

(a) (b)

Fig. 5. Pressure mode shape for the $\mathbf{3^{rd}}$ mode $n = 0$, obtained at the frequency of 0.97 with the LOM.

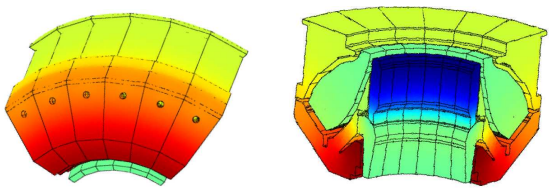

(a) (b)

Fig. 6. Pressure mode shape for the $\mathbf{7^{th}}$ mode $n = 0$, obtained at the frequency of 1.76 with the 3DFEA code.

4 A brief analysis on the effect of the mean flow

Many acoustic tools do not take into account the presence of a mean flow, and this is generally an acceptable approximation when considering only acoustic modes. Nonetheless, when combustion takes place the flame generates a streamwise pulsating *hot spot*, i.e. an entropy wave propagating at the mean flow velocity. These entropy waves could have higher amplitudes than ordinary acoustic waves [13]. Taking into account the mean flow is necessary to model entropy waves. The effect of the mean flow on the LOM results can be assessed from figure 14; it is apparent

[3] Dimensionless eigenfrequencies are obtained by scaling all the results with the lowest frequency, among all the eigenmodes obtained by the 3DFEA approach, which finds a correspondence in the LOM results.

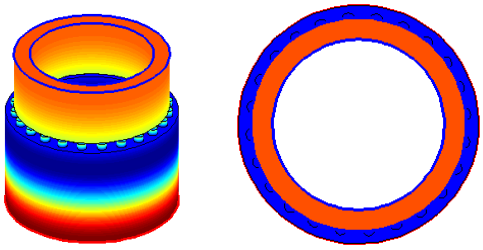

(a) (b)

Fig. 7. Pressure mode shape for the mode $n = 0$, obtained at the frequency of 1.80 with the LOM.

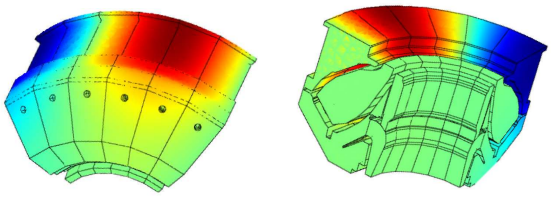

(a) (b)

Fig. 8. Pressure mode shape for the $\mathbf{10^{th}}$ mode $n = 3$, obtained at the frequency of 2.09 with the 3DFEA code.

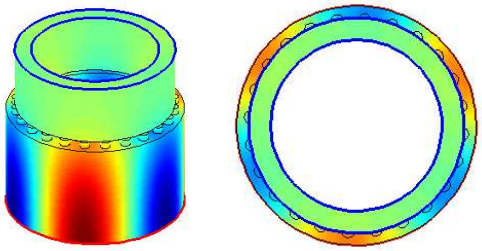

(a) (b)

Fig. 9. Pressure mode shape for the mode $n = 3$, obtained at the frequency of 2.11 with the LOM.

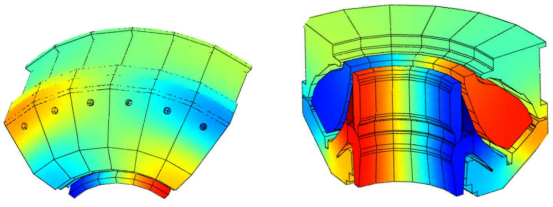

(a) (b)

Fig. 10. Pressure mode shape for the $\mathbf{13^{th}}$ mode $n = 2$, obtained at the frequency of 2.68 with the 3DFEA code.

that while for most modes the mean flow provokes damping of the mode, the frequency is but mildly affected, at least for the configuration examined here.

It has to be added that the results shown in figure 14 consider the possible presence of entropy waves in both cases. In fact, the Mach number M of the mean flow in the so-called zero-Mach case is not exactly zero, but equal to $5 \cdot 10^{-3}$ for

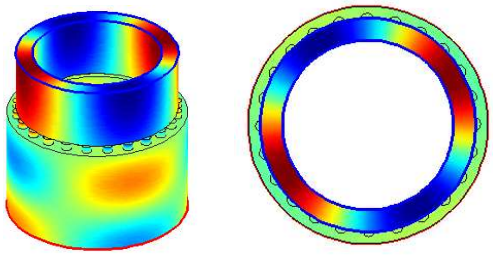

(a) (b)

Fig. 11. Pressure mode shape for the mode $n = 2$, obtained at the frequency of 2.65 with the LOM.

Table 3. List of eigenmodes obtained with the LOM and with the 3DFEA.

Mode	3DFEA	LOM	Mode	3DFEA	LOM
1	0.73	-	**9**	2.08	2.08
2	0.83	-	**10**	2.09	2.11
3	1	0.97	**11**	2.29	-
4	1.22	0.77	**12**	2.61	-
5	1.46	1.46	**13**	2.68	2.65
6	1.61	1.45	**14**	2.72	2.77
7	1.76	1.80	**15**	2.80	2.72
8	2.08	2.12	**16**	2.86	-

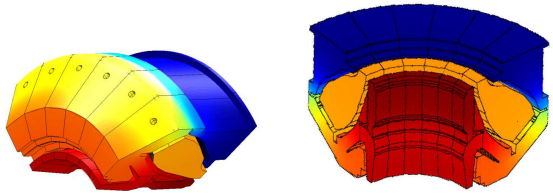

(a) (b)

Fig. 12. Pressure mode shape for the axial mode, obtained at the frequency of 0.73 with the 3DFEA code.

computational convenience. If the case $M = 0$ were computed, a few modes, corresponding to *hot spots*, would disappear.

5 The transfer function

Several transfer functions have been tested in low order models based on different approaches [2, 10, 18, 19]. Two classical transfer functions are:

$$\frac{Q'}{\bar{Q}} = \kappa \frac{m_2'}{\bar{m}_2} e^{-i\omega\tau} \tag{14}$$

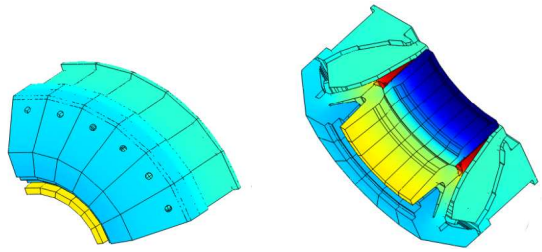

(a) (b)

Fig. 13. Mode shape for the mode obtained at 2.29 with the 3DFEA code.

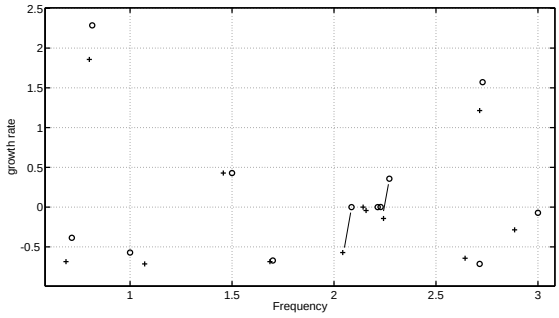

Fig. 14. **o**: zero-Mach simulation (in reality $M = 0.005$). $+$: simulation with the real Mach number of a flow evolving in a gas turbine burning system $M = 0.15$. FTF chosen: equation (15). $\kappa = 1$, $\tau = 7ms$.

$$\frac{Q'}{\bar{Q}} = \kappa \frac{u_2'}{\bar{u}_2} e^{-i\omega\tau} \tag{15}$$

The crucial weakness of these approaches is the evaluation of the unknown parameters $\kappa - \tau$. A new transfer function based on empirical data has been developed based on first principles and is hereinafter described.

5.1 Derivation of a new model

It is important to stress a consequence of the lumped approximation: the flame is located at the interface between the end of the premixers and the combustion chamber inlet as shown in figure 15(a). Comparing this model with reality, it is straightforwardly deduced what the LOM's premixer duct are modelling: the volume of flow exiting the real premixer does not immediately burn when entering the combustion chamber but it takes a short time to reach ignition thank to the recirculating flow in the inner and in the outer part of the lobed flame. In the LOM the value at the flame front are already available and the premixer in figure 15(a) represents the entire cyan-colored volume in figure 15(b).

The heat release per unit of area Q is:

$$Q = \frac{\dot{m}_F H_i}{A_{flame}}, \tag{16}$$

where $\dot{m}_F$ is the fuel mass flow rate, A_{flame} is the flame

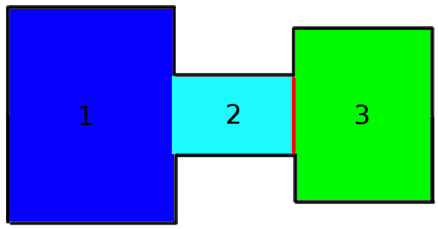

(a)

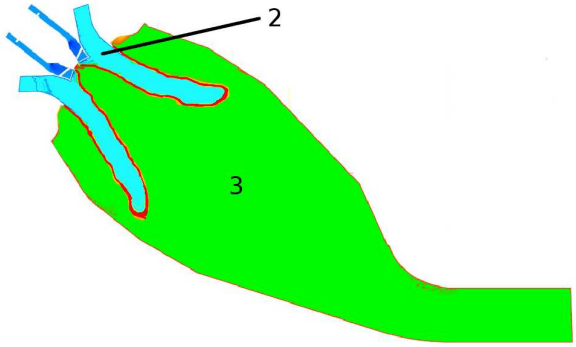

(b)

Fig. 15. (a): LOMTI's model. (b): realistic configuration. In cyan (2) the premixer is shown , in green (3) the combustion chamber, in red the flame front at their interface. The *plenum* is not represented in figure (b).

bounding area and H_i is the lower heat of combustion. Since in the lumped approximation the flame is actually located at the combustion chamber interfaces with each burner, and the thermodynamic variables of the combustion chamber are tuned in order to match the empirical flame temperature, A_{flame} is assumed equal to $A_3 = 2\pi R_3 d_3$ at the combustion chamber inlet section. This is a strong hypothesis which does not adhere to the effective flame shape; a multiplicative factor could be introduced to mitigate the effect of this assumption. Imposing

$$\dot{m}_{flame} = \dot{m}_{air} + \dot{m}_F = \rho_{flame} u_{flame} A_{cc}, \tag{17}$$

and defining the air/fuel ratio $\alpha = \dot{m}_{air}/\dot{m}_F$, an expression for Q is deduced:

$$Q = \frac{H_i \rho_{flame} u_{flame}}{\alpha + 1}. \tag{18}$$

All quantities are evaluated at the combustion chamber inlet where the flame is actually located in the present model. Operating the usual decomposition and linearising:

$$\frac{Q'}{\bar{Q}} = \frac{\rho'_{flame}}{\bar{\rho}_{flame}} + \frac{u'_{flame}}{\bar{u}_{flame}} - \frac{\alpha'}{\bar{\alpha}+1}. \tag{19}$$

Density and velocity are already present in the LOM. This is not the case for the air/fuel ratio at the combustion chamber inlet. The fluctuation of α is driven by the pressure fluctuations at the fuel injectors that are located in the middle of each diagonal swirler. Henceforth, the air/fuel ratio perturbation at the flame is related to the pressure perturbation at the orifice of each injector. This value should be phase-shifted by the time the signal takes to travel from the injectors to the flame: $e^{-i\omega\tau(f)}$. The pressure of the fuel supply ducts can be assumed constant and independent from the pressure perturbations of the air flow. Therefore, the air/fuel ratio at the injectors is linked to the fuel and air pressures according to Dalton's law of partial pressures which, for fuel and air, reads: $p_{total} = p_F + p_{air}$, or $y_F = p_F/p_{total}$ where p_{total} is the mean pressure at the injector itself, i.e. the mean pressure in each premixer duct (p_2).

Since the thermal power produced by the flame is completely converted in enthalpy of the mixture (for a perfect efficiency of the process), neglecting kinetic energy, it results $\dot{m}_F H_i \simeq \dot{m}_F(\alpha+1)c_P(T_{cc} - T_{premixer})$. The methane heat of combustion is approximately $50MJ/Kg$ and temperatures are known, so that a value $\alpha \approx 35$ is obtained. This value confirms the chemical approach that imposes a lean combustion where the equivalence ratio is set approximately to $\phi \simeq 0.53$. In this case Φ is defined as α_{ST}/α where, for the representative reaction:

$$C_xH_y + (x+\frac{y}{4})(O_2 + \frac{79}{21}N_2) \rightarrow$$
$$xCO_2 + \frac{y}{2}H_2O + (x+\frac{y}{4})\frac{79}{21}N_2,$$

a stoichiometric air/fuel ratio like

$$\alpha_{ST} = \left(x+\frac{y}{4}\right)\frac{100}{21}\frac{PM_{air}}{PM_{C_xH_y}},$$

results. For the combustion of methane in air $\alpha_{ST} \simeq 17.167$, thus

$$\alpha = \frac{\dot{m}_{air}}{\dot{m}_F} = \frac{\alpha_{ST}}{\Phi} = \frac{17.167}{0.53} \simeq 32.$$

Knowing α, it is possible to define the value of p_F that is considered unaffected by any fluctuation. Replacing values with their mean quantities:

$$\alpha = \frac{\dot{m}_{air}}{\dot{m}_F} = \frac{n_{air}}{n_F}\frac{PM_{air}}{PM_F} = \frac{p_{air}}{p_F}\frac{PM_{air}}{PM_F} =$$
$$\frac{p_{total} - p_F}{p_F}\frac{PM_{air}}{PM_F} = \left(\frac{p_2}{p_F} - 1\right)\frac{PM_{air}}{PM_F}.$$

Imposing $\chi = PM_{air}/PM_F = 1.8025$ for methane[4], the expression

$$p_F = \bar{p}_2\frac{\chi}{\chi+\bar{\alpha}}$$

results which shows that the partial pressure of the fuel is about 20 times smaller than the mean pressure of the air in the premixers. To relate pressure fluctuations at the injector to the air/fuel ratio fluctuations, using

$$\alpha = \left(\frac{p_2}{p_F} - 1\right)\chi,$$

after the usual decomposition it follows

$$\alpha' = (\chi+\bar{\alpha})\frac{p'_{inj}}{\bar{p}_2}, \tag{20}$$

where the subscript *inj* denotes the injection point.

It is possible to briefly discuss on the physical meaning of equation (20) arguing that a positive value for p', i.e. a pressure increase of the mixture in the premixer, yields a small fuel mass flow rate ensuring an increased air/fuel ratio, i.e. a positive value for α'. The value of α' already obtained reaches the flame, i.e. the combustion chamber inlet in the LOM, after a convective time delay represented by $e^{-i\omega\tau}$. The final expression for the proposed transfer function is then:

$$\frac{Q'}{\bar{Q}} = \frac{\rho'_{flame}}{\bar{\rho}_3} + \frac{u'_{flame}}{\bar{u}_3} - \frac{\bar{\alpha}+\chi}{\bar{\alpha}+1}\cdot\frac{p'_{inj}}{\bar{p}_2}e^{-i\omega\tau}. \tag{21}$$

It is remarkable the fact that $(\bar{\alpha}+\chi)/(\bar{\alpha}+1)$ is approximately equal to one in the case of lean combustion of methane and air. This term takes the place of the unknown parameter κ in equations (14) and (15). Although there is now a known multiplying factor, the presence of the time delay τ appears – so far – to be unavoidable.

The weakness of the present flame model is that of considering a flat region of heat release confined in a thin sheet at

[4] $PM_{air} = 0.21PM_{O_2} + 0.79PM_{N_2} = 0.21\cdot 32Kg\cdot mol^{-1} + 0.79\cdot 28Kg\cdot mol^{-1} = 28.84Kg\cdot mol^{-1}$, $PM_F = PM_{CH_4} = 1\cdot 12Kg\cdot mol^{-1} + 4\cdot 1Kg\cdot mol^{-1} = 16Kg\cdot mol^{-1}$

the premixers/combustion chamber interface. This is a common assumption in LOM. An alternative volumetric flame approach has been proposed in [10]. The additional hypothesis made is that of considering the fuel pressure independent from the unsteady flow field at the injectors. This is probably an acceptable approximation, considering the mechanism of fuel supply that consists in a rotating valve modulating the mass flow rate of fuel injected in the diagonal swirlers.

6 Results for a realistic turbine

A simulation on a realistic configuration can now be carried out, taking into account the mean flow and the presence of 20 adjacent *CBO*'s. Since axisymmetry is theoretically disrupted by the presence of the *CBO*'s, eigenmodes can no longer be easily recognizable as pure modes of oscillation. Actually, the *CBO*'s do not have a crucial influence on axisymmetry; the annular layout of the chambers prevails and quasi-pure eigenmodes are often recognizable.

In the literature, the specific heats C_p and C_v are generally approximated as independent from temperature. The specific heat ratio γ appears both in the mean flow computations and in the disturbance equations, when the speed of sound has to be evaluated in each duct j, as $c_{sj} = \sqrt{\gamma R T_j}$. From polynomial approximation of experimental data an expression for γ as function of the temperature T (pressure dependence is negligible) [20] can be deduced. Thus γ is not constant in the present computations, and an expression $\gamma_j = f(T_j)$ is adopted in each duct [21]. As γ goes from 1.4 to 1.3 as the temperature increases, a variation of c_s like $1 - \sqrt{1.3/1.4}$ is expected. The variation in the speed of sound affects eigenmodes, since acoustic perturbations will be slower in ducts with higher temperature (such as the combustion chamber).

6.1 Low frequency results: axial and span-wise modes

In figure 16 results for the transfer function (21) are shown. Only two unstable eigenmodes are found at dimensionless frequency equal to 1.47 and 2.71 (shown in figure 17). Importantly, they are only mildly affected by variations in τ.

The weak dependence on τ can be explained analysing the pressure mode shape in each premixer: p' does not vary significantly along the ducts, hence a reference point located in the middle of the duct experiences very similar pressure oscillations if compared to another one at any other location.

It is remarkable the fact that only two unstable modes arise, as also indicated by the experimental results available [19]. Furthermore, the two frequencies observed and measured are very close to the unstable frequencies computed in the LOM.

The weak effect of τ suggests that p'_2 has a lower influence than $\dot{m}'_3$, i.e. even if pressure perturbations at the injectors modify the equivalence ratio of the mixture, the heat release at the flame is primarily influenced by the overall mass

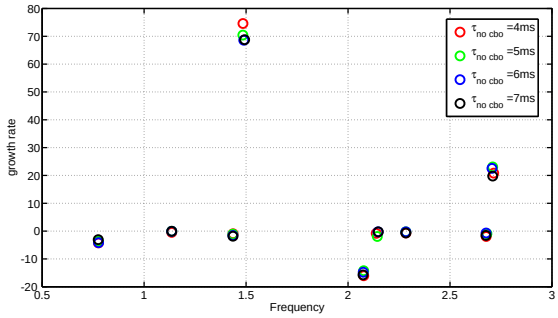

Fig. 16. Results for $L_{inj} = \frac{1}{2} L_{premixer}$, where L_{inj} means the location inside the premixers where the pressure perturbation p_{inj} is calculated. A configuration with 20 *CBO*'s is chosen. The acoustic boundary conditions are $u' = 0$. τ_{nocbo} is the value of the time delay in the burners without *CBO*'s. The value of τ in the burners with *CBO*'s has been set as $\tau_{cbo} = \tau_{nocbo} + L_{2b}/\bar{u}_2 b$.

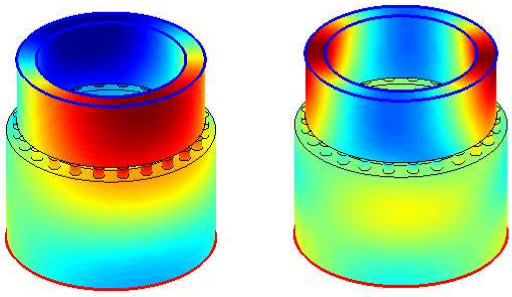

(a) (b)

Fig. 17. Pressure mode shape for the two unstable eigenmodes with $1.47 + i70\,s^{-1}$ and $2.71 + i23\,s^{-1}$, respectively.

flow rate of the fuel reaching the flame front. The resulting simplified transfer function is:

$$\frac{Q'}{\bar{Q}} = \frac{\rho'_{flame}}{\bar{\rho}_3} + \frac{u'_{flame}}{\bar{u}_3}, \tag{22}$$

and corresponding results are shown in figure 18. The unstable modes are only slightly influenced by this simplification. These results confirm the hypothesis just outlined, providing also the important conclusion that the time delay τ is not needed.

6.2 High frequency results: radial modes

As detailed in [2], modes with radial wave number m propagate in duct j only for frequencies higher than

$$f_c = \frac{\overline{c}_{sj}}{2\pi} \lambda_{m,n} \sqrt{1 - M_j^2}$$

where c_{sj} and M_j are respectively the speed of sound and the Mach number in the duct j and $\lambda_{m,n}$ is obtained from $\frac{dJ_n}{dr}(\lambda_{m,n} R) = 0$. These cut-off frequencies are given in table 6.2.

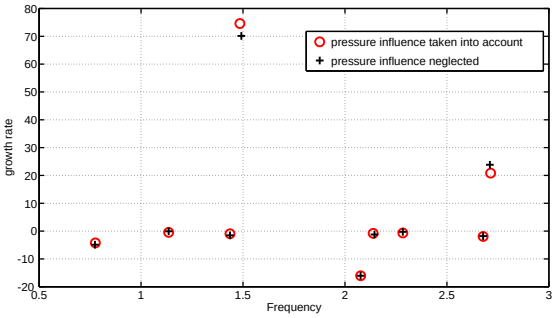

Fig. 18. Comparison between results for $\tau = 4ms$ (o) in figure 16 and the simplified transfer function (22) (+).

n	*plenum*	chamber
0	8.37	15.65
± 1	8.40	15.69
± 2	8.48	15.82

Table 4. Cut-off frequencies as function of the azimuthal wave number n for radial mode $m = 1$

Results for $m > 0$ confirm the damping phenomenon of the duct. For example in figures 19 to 21 the lowest frequencies of oscillation in the *plenum* for $n = 0, 1, 2$ and $m = 1$ are shown. From [22] it is known that radial modal coupling could be neglected since it is numerically found that, while each individual resonant frequency is slightly influenced by the other modes, the overall trends are but mildly affected: the envelops of solutions, and hence the most unstable frequencies, are essentially unaltered.

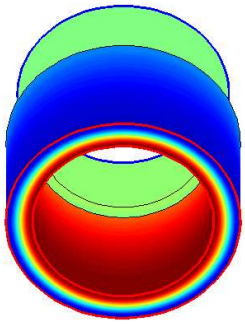

Fig. 19. Mode shape for $m = 1$ and $n = 0$ at frequency of 8.39, $GR = 1.7s^{-1}$

It is remarkable the fact that the frequencies of all these modes are slightly larger than the relative cut-off frequency. This is very comfortable since it implies that they can be safely disregarded. On the other hand, it is important to be able to account for them, since they might be related to a phenomenon known as screech. While the screech is not important in annular combustion chambers it assumes relevance when cylindrical chambers are considered.

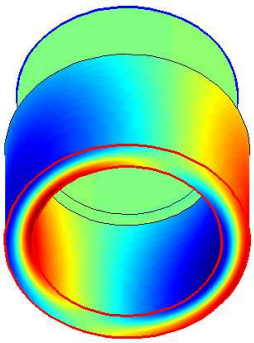

Fig. 20. Mode shape for $m = 1$ and $n = 1$ at frequency of 8.41, $GR = 1.75s^{-1}$

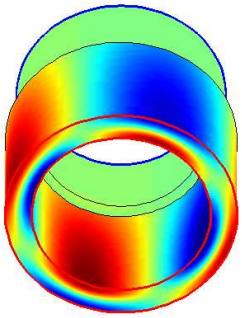

Fig. 21. Mode shape for $m = 1$ and $n = 2$ at frequency of 8.50, $GR = 1.8s^{-1}$

7 Conclusions

A low order model able to represent a network of annular and cylindrical ducts has been developed. This tool, based on the convective inhomogeneous wave equation, is able to take into account a mean flow evolving in the system as well as to model the presence of entropy waves generated by the flame. Furthermore it can easily include a vorticity term (not shown here). The lumped geometry has been calibrated against a finite element simulation by matching the acoustic modes obtained without mean flow and heat release fluctuations. The description of the calibration represents one of the achievements of the present work. The good agreement between the LOM and the 3DFEA, considering the modes suspected to yield humming, allows to recommend the further development of this model as a predictive tool capable to quickly perform those parametric studies needed in the preliminary design phase of gas-turbine burners.

It has been shown that the effect of the mean flow is important, but not critical when looking at the general behaviour. In order to find out whether a mode can become unstable, convective terms must be included. Furthermore the LOM requires the presence of a mean flow if there is the need to consider the entropy waves evolving in a non-isentropic field [13]. As a side benefit, the presence of a non-zero mean flow accelerates convergence of the numerical calculations.

A well-known transfer function has initially been used to model the flame response and the critical influence of the unknown parameters has been pointed out. Then, a new model for the flame response, coherent with the lumped approximation, has been proposed. This model still considers a steady thin flat flame located at the junction of each premixer duct with the combustion chamber, but the heat release fluctuations is deduced from well known laws. With the new model proposed here, the effect of the time lag τ on the eigenmodes is virtually absent, at least for the configuration examined, and this opens interesting perspectives for the development of new flame transfer functions based on the principles outlined here.

When looking at radial modes the LOM results confirm that screech is not critical in annular combustion chambers, whenever the azimuthal dimensions prevail over the axial ones. Nonetheless, such a phenomenon assumes a significant role when dealing with cylindrical combustion chambers where the mean thickness is no longer negligible when compared to the mean radius.

Acknowledgements

The work is part of a large-scale project by Ansaldo Energia to develop techniques to control humming. Many interactions with Andrea Di Vita (Ansaldo Energia), Giovanni Campa and Sergio Camporeale (Politecnico di Bari) are gratefully acknowledged.

References

[1] Rayleigh, L., 1896. *The Theory of Sound*. McMillan.

[2] A.P.Dowling, and S.R.Stow, 2005. "Acoustic Analysis of Gas-Turbine Combustor". *Journal of Propulsion and Power,* **19**(13), pp. 369–410.

[3] B.Schuermans, 2003. "Modelling and control of thermoacoustic instabilities". Ph.D. Thesis, École Polytechnique Fédérale de Lausanne.

[4] Sattelmayer, T., 2003. "Influence of the combustor aerodynamics on combustion instabilities from equivalence ratio fluctuations". *ASME Journal of Engineering for Gas Turbines and Power,* **125**(1), pp. 11–19.

[5] Evesque, S., and Polifke, W., 2002. "Low-order acoustic modelling for annular combustors: validation and inclusion of modal coupling". *ASME GT2002-30064*.

[6] J.W.Rumsey, M.Fleifil, A.M.Annaswamy, and A.F.Ghoniem, 1998. Low-order nonlinear models of thermoacoustic instabilities and linear model-based control. Progress report No. 9801, MIT, Cambridge, MA.

[7] Morgans, A., and Stow, S., 2007. "Model-based control of combustion instabilities in annular combustors". *Combustion and Flame,* **150**(4), pp. 380–399.

[8] Bellucci, V., Schuermans, B., Nowak, D., Flohr, P., and Paschereit, C. O., 2005. "Thermoacoustic Modeling of a Gas Turbine Combustor Equipped With Acoustic Dampers". *ASME Journal of Turbomachinery,* **127**(2), pp. 372–379.

[9] L.Crocco, and S.I.Cheng, 1956. *Theory of Combustion Instability in Liquid Propellant Rocket Motors*. Butterworths, London.

[10] Howe, M. S., 1979. "On the Theory of Unsteady High Reynolds Number Flow Through a Circular Aperture". *Proceeding of the Royal Society of London,* **366**(1725), pp. 205–223.

[11] A.Guaus, 2009. Implementation in LOMTI of a model of the Sesta's burner. Progress report, University of Genoa.

[12] H.Chanson, 2004. *Hydraulics of open channel flow: an introduction (2nd edition)*. Butterworths-Heinemann.

[13] Nicoud, F., and Poinsot, T., 2005. "Thermoacoustic instabilities: Should the Rayleigh criterion be extended to include entropy changes?". *Combustion and Flame,* **142**, pp. 153–159.

[14] Marble, F. E., and Candel, S. M., 1977. "Acoustic disturbance from gas non-uniformities convected through a nozzle". *Journal of Sound and Vibration,* **55**(2), pp. 225–243.

[15] Stow, S. R., Dowling, a. P., and Hynes, T. P., 2002. "Reflection of circumferential modes in a choked nozzle". *Journal of Fluid Mechanics,* **467**, pp. 215–239.

[16] Guaus, A., Favier, J., Bargiacchi, M., and Bottaro, A., 2011. "A quantitative comparison betewwn a Low Order Model and a 3D FEM code for the study of thermoacoustic combustion instabilities". *ASME paper GT-2011-45969*.

[17] G.Campa, and S.Camporeale, 2010. Calcolo acustico camera anulare attuale. Technical report, Politecnico di Bari.

[18] Zhu, M., Dowling, A. P., and Bray, K. N. C., 2005. "Transfer Function Calculations for Aeroengine Combustion Oscillations". *ASME Journal of Engineering Gas Turbines and Power,* **127**(1), pp. 18–26.

[19] M.Bargiacchi, 2010. "Analysis and Control of Thermoacoustic Instabilities in Gas Turbine Systems". M.S. Thesis, University of Genoa.

[20] Ceviz, M. A., and Kaymaz, I., 2005. "Temperature and air–fuel ratio dependent specific heat ratio functions for lean burned and unburned mixture". *Energy Conversion and Management,* **46**, pp. 2387–2404.

[21] *http://webbook.nist.gov/chemistry/*.

[22] Akamatsu, S., and Dowling, A. P., 2001. "Three Dimensional Thermoacoustic Oscillation in a Premix Combustor". *ASME paper GT-2001-0034*.